

Speciation and Transformation of Sulfur in Freshwater Sediments: a Case Study in Southwest China

Jingfu Wang · Jingan Chen · Jianyang Guo ·
Zhihui Dai · Haiquan Yang · Yilong Song

Received: 14 July 2017 / Accepted: 12 September 2017 / Published online: 22 September 2017
© Springer International Publishing AG 2017

Abstract Sulfur (S) is one of the most redox-sensitive elements and has a marked impact on the geochemical cycling of biogenic elements in freshwater sediments. Current understanding of the speciation of sedimentary S, and of the processes regulating it, is insufficient. In this study, the speciation and spatial variations of S and iron (Fe) in sediments (soils) from Lake Hongfeng, one of the largest freshwater lakes in Southwest China, were investigated using X-ray absorption near-edge structure (XANES) spectroscopy and diffusive gradient in thin film technique (DGT). The results show that S in sediments and soils was composed of seven fractions in different electronic oxidation states (EOSs), including (i) reduced S (R-S, G1, EOS = -1), (ii) lowly oxidized S (LO-S, including G2-G5; EOS = 0, 0.5, 2, and 3.7), and (iii) highly oxidized S (HO-S, including G6 and G7;

EOS = 5 and 6). Proportional differences of S speciation in sediments and soils indicated that HO-S is largely reduced to LO-S and R-S during depositional processes. The HO-S fraction decreased in the top surface sediments and then increased in the deeper layers, whereas the R-S fraction showed the opposite trend, suggesting that sulfate reduction and re-oxidation processes occurred in the sediments. High ratios of soluble Fe/S provided a favorable foundation for the reduction and burial of sedimentary S. The speciation and spatial variations of S in freshwater sediments are controlled by complex environmental factors, including terrigenous material discharges, water redox conditions, and porewater chemistry (such as for pH, Eh, and reactive Fe). Our study will help to deepen the understanding of the geochemical dynamics of S in the sediments of freshwater ecosystems.

Electronic supplementary material The online version of this article (<https://doi.org/10.1007/s11270-017-3580-5>) contains supplementary material, which is available to authorized users.

J. Wang · J. Chen (✉) · J. Guo · H. Yang
State Key Laboratory of Environmental Geochemistry, Institute of
Geochemistry, Chinese Academy of Sciences, Guiyang 550002,
People's Republic of China
e-mail: chenjingan@vip.skleg.cn

Z. Dai
State Key Laboratory of Ore Deposit Geochemistry, Institute of
Geochemistry, Chinese Academy of Sciences, Guiyang 550002,
People's Republic of China

Y. Song
Institute of Surface Earth System Science, Tianjin University,
Tianjin 300072, People's Republic of China

Keywords Sulfur · Iron · K-edge XANES · DGT ·
Freshwater sediments

1 Introduction

Sulfur (S), one of the most redox-sensitive elements in sediments, is of great concern in aquatic ecosystems due to its impacts on the geochemical cycling of biogenic elements (Canfield et al. 1993; Chambers et al. 2000; Couture et al. 2010). Sediments are an important sink for S, and microbially mediated sulfate reduction is postulated to be a key process in sediments (Jørgensen 1990; Choi et al. 2006). Sedimentary S can be reduced to be

sulfides either chemically or biologically under anaerobic condition, or even converted to pyrite and buried permanently (Holmer and Storkholm 2001). In addition, various intermediates, such as elemental S, organic polysulfides, and sulfonates, are generated during chemical and biological processes, although their turnover rates are high and their levels are very limited (Kohnen et al. 1989; Vairavamurthy et al. 1994; Couture et al. 2010). Therefore, further insight into the speciation of S in sediments is helpful for improving our understanding of the geochemical cycling of S.

S in sediments is usually separated into acid-volatile sulfide, elemental S, and pyrite-S, based on sequential extraction (Fossing and Jørgensen 1989; Wijsman et al. 2001). This methodology can, to a certain extent, help us understand the nature of S in sediments. However, it is a considerable challenge to precisely explain the analyzed results because of the following: (1) artifacts cannot be avoided during sequential extraction due to sample integrity loss and reagent selectivity (Prietz et al. 2003) and (2) speciation of S provided by sequential extraction is the geochemical form rather than the chemical form, making it very difficult to establish a reaction mechanism. Until now, little is known about the chemical forms of S in sediments due to a lack of sensitive analytical methods (Luther et al. 2001).

Fortunately, the development of modern analytical techniques makes it possible to determine the chemical forms of S. Synchrotron-based X-ray absorption near-edge structure (K-edge XANES) spectroscopy has become a sensitive and nondestructive method for probing the electronic structure and chemical forms of elements in natural matrixes (Jalilvand 2006). XANES has recently been successfully used to identify the chemical forms of S in soil and marine sediments (Xia et al. 1998; Prietz et al. 2010; Solomon et al. 2011; Zeng et al. 2013). Furthermore, a high resolution passive sampling technique, namely the diffusive gradient in thin films technique (DGT), was developed based on Fick's first law (Davison and Zhang 1994). DGT was initially designed as an in situ and high-resolution method for the measurement of heavy metals (Stockdale et al. 2009; Panther et al. 2014). It has now become a powerful tool with the potential to simultaneously measure S and related heavy metals (e.g., Fe) at a millimeter resolution (Naylor et al. 2004; Ding et al. 2012; Xu et al. 2013), using a combined DGT probe containing a layer of AgI and a layer of chelating resin. XANES

combined with DGTs could be an efficient combination for the investigation of S in sediments.

Lake Hongfeng is one of the largest freshwater lakes in Southwest China. It has suffered eutrophication problem for more than 10 years, which is the major threat facing by freshwater lakes in China. Phosphorus (P) is the primary nutrient governing the trophic status of lakes. The release of P from sediments has become the major source of P, resulting in an increased risk of eutrophication in this lake (Wang et al. 2016). Internal-P release is assumed to be a coupled process associated with the geochemical cycling of S and Fe (Jensen et al. 1992; Ding et al. 2012). However, current knowledge of the speciation of S (Fe) in the sediments is very limited. In this study, K-edge XANES combined with DGT was employed to determine the chemical forms of S (Fe) in the sediments. The aims of the present work are (1) to obtain a high-resolution record of S species in freshwater sediments and (2) to address the transformation processes of S in freshwater sediments.

2 Materials and Methods

2.1 Study Site

Lake Hongfeng (106.24° E, 26.32° N) has a surface area of 57.2 km², a mean depth of 10.5 m, and a storage capacity of 6.01×10^8 m³ (Fig. 1). It is a seasonal hypoxic water body that is heavily polluted by P, nitrogen (N), and organic matter (OM). Concentrations of total P (TP), total N (TN), and total organic carbon (TOC) in surface sediments are in the range of 766–4306 mg/kg (mean: 1815 mg/kg), 0.27–0.78% (mean: 0.38%), and 1.99–10.62% (mean: 3.97%), respectively ($n = 107$, unpublished data). The water columns are strongly stratified in summer, and bottom waters are anaerobic (DO < 0.5 mg/L) for more than 120 days per year (Wang et al. 2016).

2.2 Sample Collection

Sediment cores were collected from south central (SC) and north central (NC) in Lake Hongfeng using a gravity corer (6 cm i.d.) in July 2013. Upon collection, sediment cores were sealed and immediately wrapped in tinfoil and were then transported to the laboratory as soon as possible. Water temperature (T), pH, and

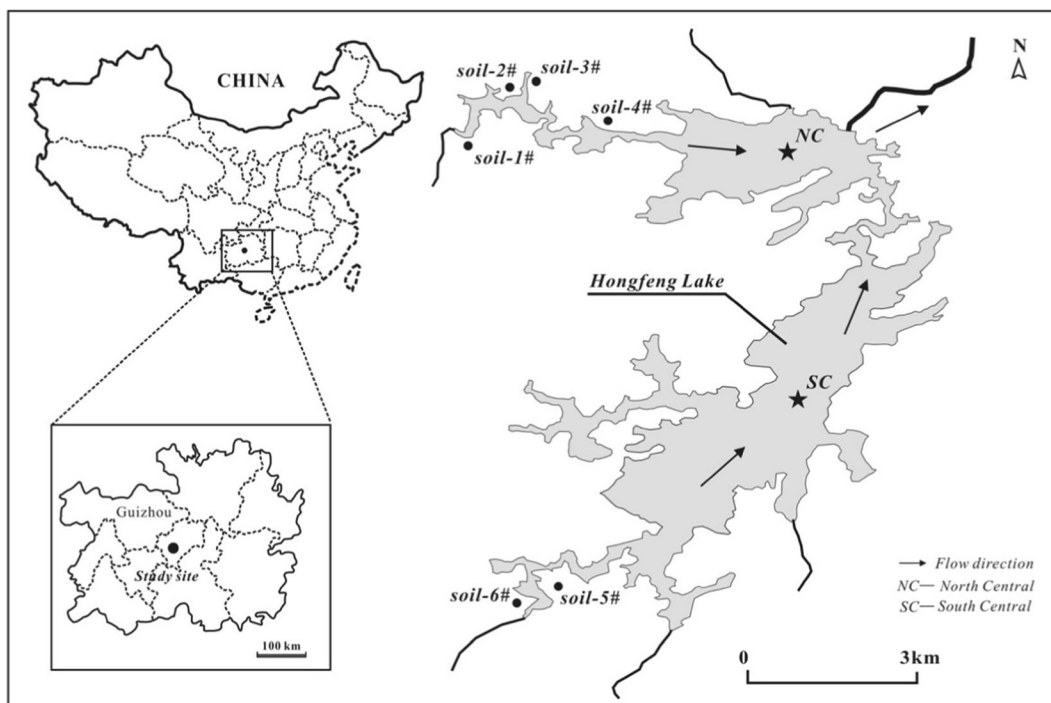


Fig. 1 Map of the study area

dissolved oxygen (DO) in the water column were determined in situ using a multi-parameter water quality sonde (YSI 6600V2) at a 1-m interval. Six soil samples were collected from the fluctuating zone along the two major inflows, i.e., the Yangchang river and Taohuayuan river. Soil samples were put into plastic sealing bags and transported to the laboratory. After microsensor and DGT measurements, sediment cores were sliced into 2-cm sections under N_2 atmosphere. The sediment and soil samples were freeze-dried, sieved, and then stored at 4 °C until K-edge XANES and chemical analysis.

2.3 Microsensors and Measurements

The pH and redox potential (Eh) of pore water were measured using a versatile four-channel Microsensor Multimeter (Unisense, Science Park Aarhus, Denmark) with a high resolution of 300 μ m. The pH microelectrode is a miniaturized glass pH electrode that must be calibrated with standard pH buffers before use. It is under a response time of less than 20 s in most cases (90%). The redox microelectrode is a miniaturized platinum electrode. Before measurements, the reference electrode should be calibrated with quinhydrone redox buffer (pH 4 and 7).

2.4 DGT Analysis

ZrO-Chelex and ZrO-AgI DGT probes (Easysensor Ltd., Nanjing, China) were used to measure dissolved Fe(II) (DGT-Fe) and dissolved S(-II) (DGT-S). Prior to measurement, DGTs must be deoxygenated with nitrogen overnight and then bound back to back. After being inserted into the sediments for 24 h and then retrieved, ZrO-Chelex binding gels were sliced at 2-mm intervals along the vertical direction, and each slice was eluted with 1.0 M HNO_3 . Soluble Fe in the eluents (DGT-Fe) was determined using an Epoch Microplate Spectrophotometer (BioTek, Winooski, VT) (Laskov et al. 2007; Xu et al. 2013). ZrO-AgI binding gels were scanned using a flat-bed scanner (Canon 5600F) at a resolution of 300 dpi. The DGT-S concentration was determined using a computer imaging densitometry technique (Ding et al. 2012).

2.5 K-Edge XANES Analysis

K-edge XANES spectra of S were recorded at the Synchrotron Radiation Facility (beam-line 4B7A, Beijing, China). The synchrotron radiation was filtered by a monochromator equipped with Si (111) double crystals.

Spectra were scanned from 2420 to 2520 eV at a step width of 0.2 eV, in fluorescence mode using a fluorescent ion chamber Si (Li) detector (PGT LS30135). The samples were pressed into thin films before analysis. During the measurement, the incoming intensity was 1.8 GeV. The photon flux on the sample was $\sim 10^9$ photons/s. Additional filters were placed between the sample and the detector to reduce the fluorescence signal derived from Si in the samples. The X-ray energy was calibrated with reference to the spectrum of the highest resonance energy peak of ZnSO_4 at 2482.6 eV. The X-ray absorption data at the Fe K-edge of the samples were recorded in fluorescent mode using a silicon drift fluorescence detector at beam line BL14W1 of the Shanghai Synchrotron Radiation Facility (SSRF), China. The station was operated with an Si (111) double crystal monochromator. During the measurement, the synchrotron was operated at an energy of 3.5 GeV and a current between 150 and 210 mA. The photon energy was calibrated with the first inflection point of the Fe K-edge (7112 eV) in Fe foil.

Data analysis of K-edge XANES was conducted using the IFEFFIT package of Athena software (Newville 2001). Seven Gaussian (white-line) functions (G1, G2, G3, G4, G5, G6, and G7) were taken into account for the K-edge XANES of S. Two arctangent functions, representing S s/p transitions of reduced and oxidized forms of S, were applied for the fittings (Manceau and Nagy 2012; Zhu et al. 2014). With respect to the k-edge XANES of Fe, methods described elsewhere (Prietz et al. 2007) were followed. Briefly, after normalization, parameters for the pre-edge (7106–7118 eV) features were extracted by simultaneously fitting the baseline, which consisted of a damped harmonic oscillator function and two Gaussian functions to describe the pre-edge peaks. The abundance of each form of Fe was determined from their peak area.

2.6 Sediment Properties

TN and total S (TS) were measured using an elemental analyzer (Vario MACRO cube, Elementar, Germany). For TOC analysis, all samples were pretreated with 12 M HCl overnight to remove carbonates and were then measured using an elemental analyzer. After digestion with mixed acid (HNO_3 -HCl-HF), total Fe was analyzed by inductively coupled plasma/optical emission spectrometry (ICP-OES). All data were presented on a dry/wet basis.

3 Results

3.1 Water Chemistry and Sediment Properties

The water body of Lake Hongfeng has a significant thermal stratification at SC and NC. The thermocline is within the depth of 8–12 m (Fig. 2). The temperature of the bottom water is 22 °C. Concentrations of DO at SC and NC are at least 8.0 mg/L in surface water and decline sharply below a depth of 8 m. These concentrations are generally lower than 0.5 mg/L in the bottom water. pH values decline slowly with water depth, i.e., from 8.8 in the surface water to 7.8 in the bottom water.

Sediment samples are characterized by elevated TS (0.54 ~ 1.81%), TN (0.57 ~ 0.62%), and TOC (7.11 ~ 9.10%) at NC and relatively low levels of TS (0.33 ~ 0.41%), TN (0.31 ~ 0.42%), and TOC (4.05 ~ 5.88%) at SC (Table 1). TN and TOC contents are highest in the top layer at both sites and decrease with increasing water depth. TS contents are high in both surface and deep sediments and are lowest at a depth of 6–8 cm. Total Fe contents range from 2.78 to 6.92% (mean: 5.13%) at NC and from 2.15 to 11.7% (mean: 7.27%) at SC. Total Fe at both sites decreases with increasing depth. The mean values of TOC/TN (15.5) and total Fe/TS (3.2) in sediments from NC are lower than those in sediments from SC, with corresponding mean values of 16.3 and 10.8.

3.2 pH and Eh in Sediments

The pH values are in the range of 7.3 ~ 7.8 at NC, comparable to those at SC (7.2 ~ 7.9) (Fig. 3). The pH values decrease substantially within a depth of 0–1 cm at both sites but are relatively constant in the deeper layers. The Eh values are in the range of – 80 ~ 410 and – 125 ~ 270 mV at NC and SC, respectively. Drastic decreases in the Eh values also occur within a depth of 0–1 cm at both sites and then remain constant in deeper layers (~ 100 mV).

3.3 Speciation of S and Fe in Sediments

The typical K-edge XANES spectra of S and the well-fitted curves are shown in Fig. 4 (all spectra are presented in Fig. S1 and S2). There are several white lines in the XANES spectra, indicating the presence of multiple electronic oxidation states (EOSs). The relative abundance of each Gaussian curve, representing

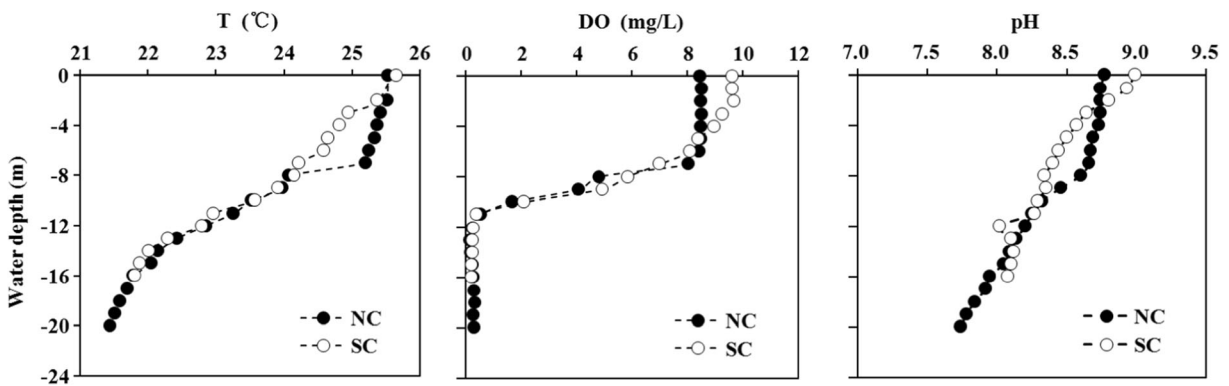


Fig. 2 Vertical profiles of temperature, dissolved oxygen, and pH in the water column

different EOSs, is displayed in Table 2. We merged these S fractions into three groups: (1) reduced S (R-S, G1, representing pyrite, EOS = - 1), (2) lowly oxidized S (LO-S, sum of G2, G3, G4, and G5, including elemental S, L-cysteine, sulfoxide, and sulfite; EOS = 0, 0.5, 2, and 3.7), and (3) highly oxidized S (HO-S, sum of G6 and G7, including sulfonate and sulfate; EOS = 5 and 6). R-S accounts for 12.2 ± 4.2 and $7.4 \pm 4.2\%$ of the total S at NC and SC (not including SC-4, 5), respectively. The relative abundance of HO-S is $36.5 \pm 5.9\%$ at NC and $28.1 \pm 7.1\%$ at SC. The abundance of LO-S gradually increases with increasing depth. The XANES spectra of S in soil is relatively simple, characterized by a low abundance of R-S (mean: $2.4 \pm 3.2\%$) and a high abundance of HO-S (mean: $43.1 \pm 5.6\%$).

The typical K-edge XANES spectra of Fe and the well-fitted curves are shown in Fig. 5 (all spectra are presented in Fig. S3). The relative abundance of Fe species is displayed in Table 3. Among the Fe species, ferrous Fe accounts for 50.4% and 47.9% of the total Fe in sediments collected from NC and SC, respectively. The fractional contribution of ferric Fe in sediments slightly decreases with increasing depth.

3.4 DGT-S and DGT-Fe in Sediments

The vertical profiles of DGT-S and DGT-Fe are shown in Fig. 6. Concentrations of DGT-S in sediments from NC are in the range of 0–0.002 mg/L and increase with sediment depth. Concentrations of DGT-S in sediments

Table 1 Total sulfur (TS, %), total nitrogen (TN, %), total organic carbon (TOC, %), and total iron (Σ Fe, %) in sediments and the ratios of TOC/TN and Σ Fe/TS

Location	TS (mean \pm SD)	TN (mean \pm SD)	TOC (mean \pm SD)	TOC/TN	Σ Fe	Σ Fe/TS
NC						
0–2 cm	0.89 ± 0.17	0.62 ± 0.00	9.10 ± 0.03	14.6	3.35	2.2
2–4 cm	1.23 ± 0.20	0.59 ± 0.01	8.49 ± 0.12	14.5	2.78	1.3
4–6 cm	0.70 ± 0.10	0.57 ± 0.02	7.53 ± 0.18	13.2	3.92	3.2
6–8 cm	0.54 ± 0.09	0.57 ± 0.01	7.11 ± 0.22	12.5	6.47	6.8
8–10 cm	0.88 ± 0.25	0.60 ± 0.00	7.57 ± 0.04	12.7	5.79	3.8
10–12 cm	1.43 ± 0.11	0.57 ± 0.00	7.61 ± 0.03	13.5	6.66	2.7
12–14 cm	1.81 ± 0.23	0.62 ± 0.01	7.55 ± 0.09	12.2	6.92	2.2
SC						
0–2 cm	0.33 ± 0.05	0.42 ± 0.01	5.88 ± 0.13	13.9	2.15	3.7
2–4 cm	0.41 ± 0.06	0.37 ± 0.01	5.54 ± 0.02	15.1	3.23	4.5
4–6 cm	0.41 ± 0.11	0.35 ± 0.00	5.17 ± 0.02	14.9	4.88	6.8
6–8 cm	0.36 ± 0.01	0.35 ± 0.01	4.96 ± 0.03	14.2	7.27	11.5
8–10 cm	0.37 ± 0.03	0.32 ± 0.00	4.87 ± 0.03	15.1	10.01	15.5
10–12 cm	0.38 ± 0.01	0.33 ± 0.00	4.39 ± 0.01	13.3	9.94	14.9
12–14 cm	0.41 ± 0.08	0.34 ± 0.00	4.07 ± 0.10	12.1	8.98	12.5
14–16 cm	0.39 ± 0.01	0.31 ± 0.00	4.05 ± 0.01	13.0	11.71	17.2

Fig. 3 Vertical profiles of pH and Eh in sediments

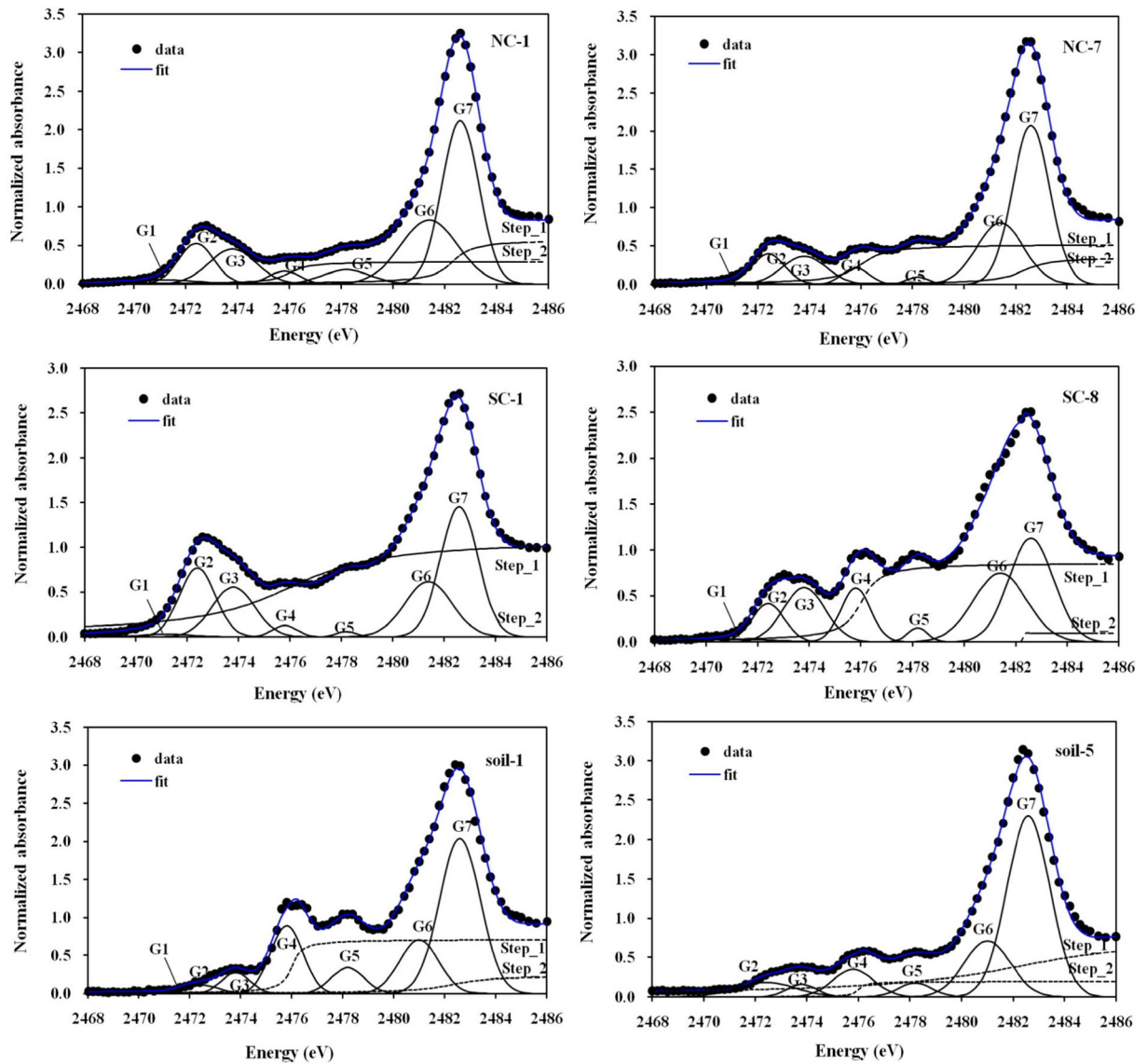
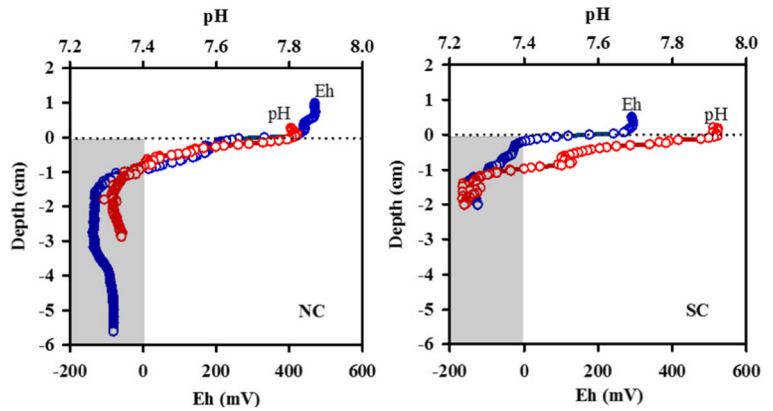


Fig. 4 Vertical profiles of DGT-S and DGT-Fe in sediments

Table 2 Abundance of different S species in sediments and soils

Samples	Abundance of each fraction (%)						GCF test		
	G1 EOS = -1	G2 EOS = 0	G3 EOS = 0.5	G4 EOS = 2	G5 EOS = 3.7	G6 EOS = 5	G7 EOS = 6	R-factor	Chi-square
NC									
0–2 cm	10.6	26.7	19.6	3.04	3.77	14.5	21.7	0.00116	0.14151
2–4 cm	9.33	34.9	28.5	0.43	0.62	16.2	10.0	0.00018	0.02214
4–6 cm	15.0	25.4	24.1	1.41	4.37	11.3	18.4	0.00019	0.02555
6–8 cm	15.4	21.5	22.4	2.45	0.56	10.9	26.8	0.00119	0.14153
8–10 cm	17.5	15.0	19.2	3.36	3.95	11.1	29.9	0.00142	0.17608
10–12 cm	12.1	21.5	19.7	5.22	0.97	12.7	27.8	0.00139	0.17011
12–14 cm	5.34	25.3	19.7	4.67	1.17	15.3	28.5	0.00150	0.18637
SC									
0–2 cm	4.82	43.0	23.5	2.00	0.54	9.67	16.4	0.00024	0.02797
2–4 cm	11.4	23.1	22.6	4.26	1.96	12.8	24.0	0.00110	0.13174
4–6 cm	8.91	23.8	25.6	5.29	1.42	12.8	22.2	0.00112	0.13259
6–8 cm	46.2	15.0	14.6	4.23	0.98	7.94	11.0	0.00064	0.07309
8–10 cm	48.6	13.1	12.6	6.91	2.34	9.21	7.26	0.00062	0.07417
10–12 cm	9.81	21.2	26.7	13.9	2.25	12.4	13.8	0.00084	0.10262
12–14 cm	7.61	18.9	20.4	14.6	3.61	16.6	18.3	0.00108	0.13604
14–16 cm	6.80	22.6	26.4	12.1	1.45	14.3	16.4	0.00123	0.15684
Soil									
1#	7.38	8.27	10.0	24.1	6.60	11.7	32.0	0.00118	0.15962
2#	ND	11.1	5.96	29.0	9.08	9.41	35.5	0.00203	0.28133
3#	ND	12.4	24.5	23.3	1.98	11.6	26.3	0.00062	0.07815
4#	1.73	15.9	15.4	21.8	4.80	12.0	28.3	0.00100	0.12892
5#	ND	23.3	6.45	12.3	3.68	14.5	39.7	0.00126	0.15747
6#	5.44	7.30	23.7	20.3	5.44	17.5	20.3	0.00092	0.11840

from SC are obviously higher than those in sediments from NC, with a peak value of ~ 0.004 mg/L corresponding to a depth of 3–5 cm and decreasing thereafter. Although concentrations of DGT-Fe at NC (0.66–4.41 mg/L) and SC (0.01–3.46 mg/L) differ, the vertical profiles of DGT-Fe are similar at both sites, with an increase within 0–5 cm and a decrease towards the deeper layers.

4 Discussion

4.1 Migration and Transformation of S in the Water and Sediments

We speculate that sedimentary S in Lake Hongfeng is largely derived from terrigenous inputs because S is usually closely bound to OM, which is predominated by terrigenous origin in Lake Hongfeng. This is supported by the ratio of TOC/TN in the sediment samples, with a mean value of 15.9 (range: 14.1–17.6) that is within the

scope of typical terrigenous sources (usually > 15) (Meyers and Ishiwatari 1993). The abundance of HO-S ($43.1 \pm 6.2\%$) in soil samples is much higher than that in surface sediments ($31.7 \pm 5.0\%$) (Fig. 7), while the abundance of LO-S ($54.4 \pm 6.1\%$) and R-S ($2.4 \pm 3.2\%$) in soil samples is much lower than that in surface sediments ($58.3 \pm 6.9\%$ and $10.0 \pm 3.3\%$). This indicates that HO-S is largely reduced to LO-S and R-S during subsidence of suspended particulates derived from soil from water surface to sediment-water interface.

On the basis of our investigations, it appears that sulfate reduction and re-oxidation of R-S occurred in the surface sediments of Lake Hongfeng. Specifically, the HO-S decreases in the surface (8–10 cm) sediments and then increases in the deeper layers, while R-S shows the opposite trend in sediment profiles of NC and SC. Sediments from SC have a relatively larger variation in extent of HO-S and R-S, as compared with those from NC. Figure 6 shows that the sediments of SC have obviously higher DGT-S compared with NC, revealing that strong sulfate reducing activities occur in the

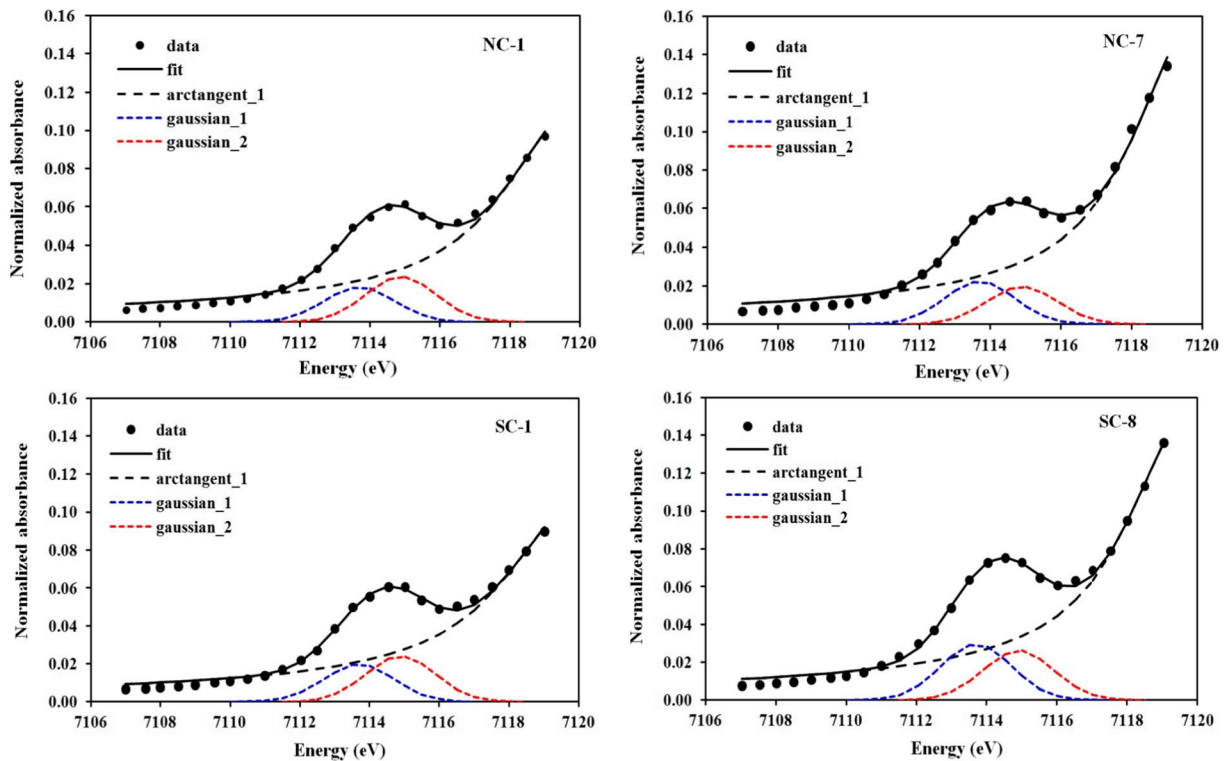


Fig. 5 K-edge XANES spectra of S and their fitted curves

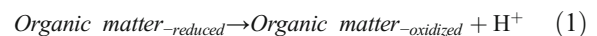
sediments of SC. This result is concordant with the above observations of the HO-S and R-S changes in the sediments.

Table 3 Abundance of Fe(II) and Fe(III) in sediments

Samples	Relative abundance (%)		Fit test	
	Fe(II)	Fe(III)	R-factor	Chi-square
NC				
0–2 cm	43.4	56.6	0.00146	0.00009
2–4 cm	51.0	49.0	0.00232	0.00020
4–6 cm	56.3	43.7	0.00287	0.00034
6–8 cm	52.0	48.0	0.00188	0.00015
8–10 cm	51.0	49.0	0.00182	0.00014
10–12 cm	45.8	54.2	0.00477	0.00010
12–14 cm	53.3	46.7	0.00209	0.00019
SC				
0–2 cm	45.0	55.0	0.00138	0.00008
2–4 cm	46.2	53.8	0.00152	0.00014
4–6 cm	44.5	55.5	0.00181	0.00015
6–8 cm	48.3	51.7	0.00132	0.00010
8–10 cm	47.1	52.9	0.00118	0.00008
10–12 cm	48.3	51.7	0.00102	0.00010
12–14 cm	51.1	48.9	0.00097	0.00009
14–16 cm	52.9	47.1	0.00095	0.00010

Trends of LO-S, including several S species, are complicated in sediments. At NC, LO-S varies vertically in a manner nearly opposite to that of HO-S. At SC, LO-S has a similar trend as HO-S. This means that in SC sediments (strongly reducing conditions), a substantial portion of HO-S and LO-S is utilized as terminal electron acceptors and these components are reduced to R-S, while in NC sediments (weak reducing conditions), HO-S reduction produces only some R-S, and most of the remaining products are LO-S.

The sediment-water interface of Lake Hongfeng must be anaerobic due to the DO level in the bottom water (less than 0.5 mg/L; Fig. 2). However, the Eh value is positive in the uppermost sediments (0–1 cm). Under the positive Eh and anaerobic conditions, the deposited OM in the reduced state is likely to be oxidized to OM in the oxidized state (Eq. 1), accompanied by the release of H⁺ (Risgaard-Petersen et al. 2012). This process logically leads to a rapid decline in pH and Eh values in the surface sediments, as illustrated in Fig. 3.



Hydrogen sulfide (H₂S) is widely accepted as an important product of the bacterially mediated reduction

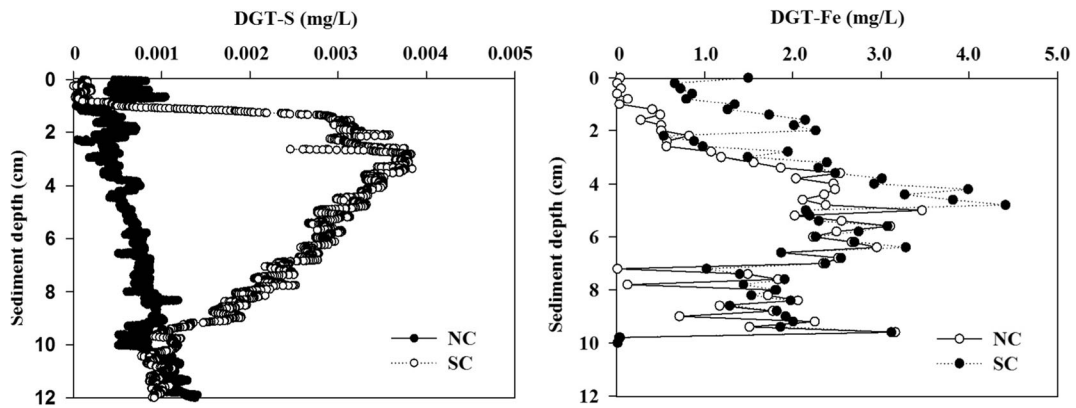


Fig. 6 K-edge XANES spectra of Fe and their fitted curves

of sulfate (Howarth 1984; Hockin and Gadd 2003). Bacteria obtain energy by oxidizing OM (Eq. 2) or molecular hydrogen (Eq. 3) using sulfate in the absence of oxygen (Muyzer and Stams 2008; Risgaard-Petersen et al. 2012). Competitive interactions in the upper sediments promote the degradation of OM (Holmkvist et al. 2011). Therefore, in the upper sediments (0–10 cm), the consumption of sulfate is responsible for the increase in the reduced and low-oxidized S fractions, following the increase in DGT-S and the decrease in TOC. According to our data, the concentration peaks of DGT-S in sediments are possibly related to this mechanism.

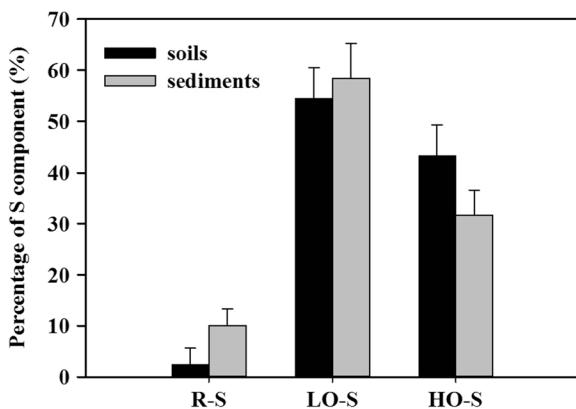
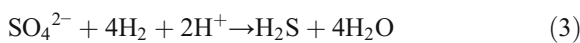
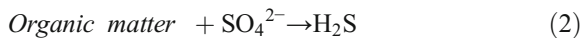


Fig. 7 Abundance of each sulfur fraction in soils ($n = 6$) and surface sediments ($n = 4$)

In the deeper sediments (> 10 cm), R-S shows a decreasing tendency at both sites, while the abundance of LO-S and HO-S dramatically increases, especially sulfate and sulfoxide (Fig. 8). This suggests that the reduction of sulfate weakens gradually, and re-oxidation of R-S occurs in the deep sediments. The transformation of S in sediments involves a complex interplay of sulfate reduction, diagenetic inter-conversion, and biogenic deposition via a dynamic cycling of diverse reduced and oxidized S forms (Urban et al. 1994; Couture et al. 2010). Sulfides can undergo re-oxidation via chemical or bacterial oxidation processes (Elsgaard and Jørgensen 1992; Holmer and Storkholm 2001). Microbial and chemical oxidation of dissolved sulfide leads to the formation of sulfur intermediates besides dissolved sulfate (Yao and Millero 1996); this is consistent with our observations in sediments of Lake Hongfeng. Interestingly, the re-oxidation process of S in deeper sediments is the exact opposite of the reduction process that soil S undergoes in the water column/sediment-water interface, suggesting that some chemical/biological responses of the sulfur cycle in deep-water ecosystems are reversible.

4.2 Influence of Fe on the Geochemical Cycling of S in Sediments

Fe is an important electron shuttle that carries electrons from the anaerobic zone to the sediment surface (Thamdrup 2000). Sediment samples from Lake Hongfeng have high concentrations of total Fe, of which 50% are ferric Fe. Under reducing conditions, ferric Fe is prone to chemical or biochemical reduction, especially when $Eh < 0$ (Stumm and Baccini 1978). The

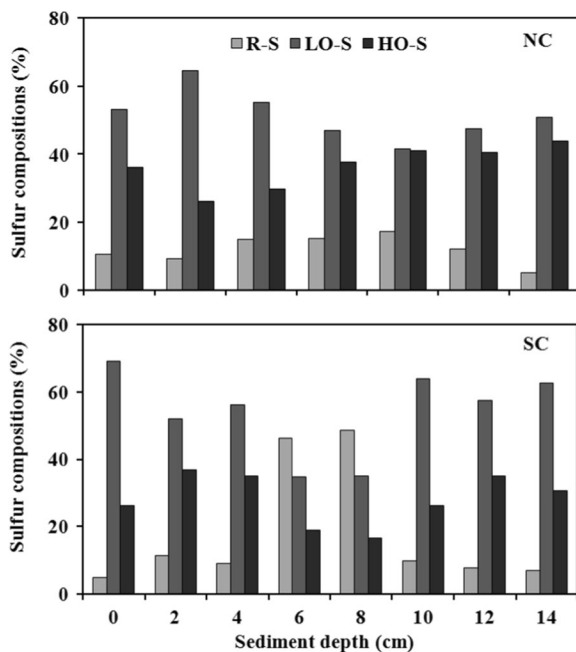


Fig. 8 Abundance of three major S groups in different EOSs (R-S, LO-S, and HO-S) in the sediment cores

XANES of Fe shows that ferrous ion slowly increases with increasing depth (Table 3), indicating that ferric Fe is partly reduced to ferrous Fe. Concentrations of DGT-Fe in surface sediments are rather high, and the maximum level reaches 4.41 mg/L at a depth of 4.8 cm at the NC site, suggesting strong Fe reduction activities in sediments.

Although there is no significant correlation between total Fe and TS (the same holds true for DGT-Fe and DGT-S), reduction of ferric Fe can potentially affect the geochemical cycling of S. Firstly, various intermediates of S (e.g., elemental sulfur and thiosulfate) and their variations are the likely products of chemical reactions between sulfide and ferric Fe (Pyzik and Sommer 1981; Jørgensen 1990; Yao and Millero 1996). Secondly, re-oxidation of R-S in deep sediments is likely enhanced by the reduction of ferric Fe, leading to an increase in sulfoxide and sulfate fractions (Fig. 8). Moreover, ratios of DGT-Fe to DGT-S in the sediments from NC and SC are much higher than 100 (Fig. 9), which is favorable for the co-precipitation of S and Fe as well as sedimentary S burial. Pyrite is a diagenetic product formed from the reaction of hydrogen sulfide with Fe minerals (Haese et al. 1997; Hansel et al. 2015). Sufficient supply of H_2S results in the formation of iron sulfide (FeS) (Luther et al. 1991; Rickard 1995), which can further react with H_2S to pyrite with the concomitant

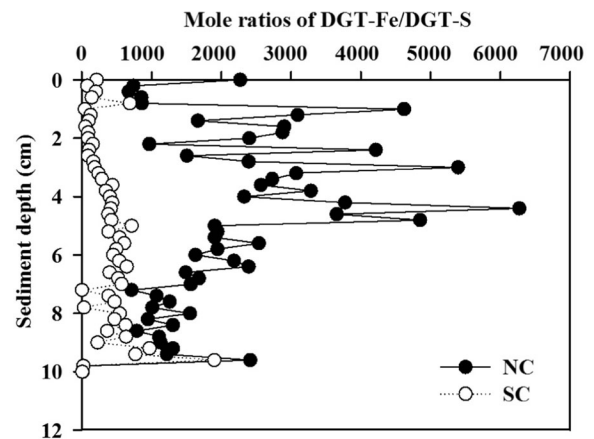


Fig. 9 Vertical profiles of the DGT-Fe/DGT-S ratios at NC and SC

formation of molecular hydrogen (Rickard 1997; Rickard and Luther 1997), resulting in elevated pyrite in the upper sediments. Co-precipitation of Fe and S likely maintains high concentrations of TS and low concentrations of DGT-S in sediments.

Within natural sediments, sulfur-fueled Fe reduction is a dominant process regardless of the Fe oxide present, while S recycling is an essential catalytic engine driving the Fe cycle (Nguyen-Thanh and Bandosz 2005). Depth distributions of various dissolved and particulate S and Fe compounds within the surface sediments can provide critical information on the early diagenetic reactions in deep freshwater ecosystems.

5 Conclusion

Sediments and soils collected from Lake Hongfeng and its catchment had the same speciation of S that included seven fractions (G1-G7) in different electronic oxidation states (EOSs). The composition of S in sediments and soils indicated that some LO-S (G4) and HO-S (G7) were reduced to other LO-S (G2, G3) and R-S (G1) when soil was introduced into the sediment. Synchronous and opposite variations of HO-S and R-S in sediments suggested the reduction and re-oxidation of S in the sediment. Trends of LO-S in sediments were more complicated than those of other S species. Under strongly reducing conditions, substantial portions of HO-S and LO-S were likely reduced to R-S, while under weak reducing conditions, most HO-S were likely reduced to LO-S. The geochemical cycling of Fe was potentially coupled with the S cycle in sediments.

Acknowledgements This work was financially supported by the National Key Research and Development Project by MOST of China (No. 2016YFA0601000), the Chinese NSF Project (No. 41403113), and the Science and Technology Project of Guizhou Province ([2015]2001). The authors thank beam-line 4B7A (Beijing Synchrotron Radiation Facility) and BL14W1 (Shanghai Synchrotron Radiation Facility) for providing the beam time.

References

- Canfield, D. E., Thamdrup, B., & Hansen, J. W. (1993). The anaerobic degradation of organic matter in Danish coastal sediments: Iron reduction, manganese reduction, and sulfate reduction. *Geochimica et Cosmochimica Acta*, *57*, 3867–3883.
- Chambers, R. M., Hollibaugh, J. T., Snively, C. S., & Plant, J. N. (2000). Iron, sulfur, and carbon diagenesis in sediments of Tomales Bay, California. *Estuaries*, *23*, 1–9.
- Choi, J. H., Park, S. S., & Jaffé, P. R. (2006). Simulating the dynamics of sulfur species and zinc in wetland sediments. *Ecological Modelling*, *199*, 15–323.
- Couture, R.-M., Gobeil, C., & Tessier, A. (2010). Arsenic, iron and sulfur co-diagenesis in lake sediments. *Geochimica et Cosmochimica Acta*, *74*, 1238–1255.
- Davison, W., & Zhang, H. (1994). In-situ speciation measurements of trace components in natural waters using thin film gels. *Nature*, *367*, 546–548.
- Ding, S., Sun, Q., Xu, D., Jia, F., He, X., & Zhang, C. (2012). High-resolution simultaneous measurements of dissolved reactive phosphorus and dissolved sulfide: The first observation of their simultaneous release in sediments. *Environmental Science & Technology*, *46*, 8297–8304.
- Elsgaard, L., & Jørgensen, B. B. (1992). Anoxic transformations of radiolabeled hydrogen sulfide in marine and freshwater sediments. *Geochimica et Cosmochimica Acta*, *56*, 2425–2435.
- Fossing, H., & Jørgensen, B. B. (1989). Measurement of bacterial sulfate reduction in sediments: Evaluation of a single-step chromium reduction method. *Biogeochemistry*, *8*, 205–222.
- Haese, R. R., Wallmann, K., Dahmke, A., Kretzmann, U., Müller, P.J., & Schulz, H.D. (1997). Iron species determination to investigate early diagenetic reactivity in marine sediments. *Geochimica et Cosmochimica Acta*, *61*(1), 63–72.
- Hansel, C. M., Lentini, C. J., Tang, Y., Johnston, D. T., Wankel, S. D., & Jardine, P. M. (2015). Dominance of sulfur-fueled iron oxide reduction in low-sulfate freshwater sediments. *ISME Journal*, *9*(11), 2400–2412.
- Hockin, S. L., & Gadd, G. M. (2003). Linked redox precipitation of sulfur and selenium under anaerobic conditions by sulfate-reducing bacterial biofilms. *Applied & Environmental Microbiology*, *69*, 7063–7072.
- Holmer, M., & Storkholm, P. (2001). Sulphate reduction and sulphur cycling in lake sediments: A review. *Freshwater Biology*, *46*, 431–451.
- Holmkvist, L., Ferdelman, T. G., & Jørgensen, B. B. (2011). A cryptic sulfur cycle driven by iron in the methane zone of marine sediment (Aarhus Bay, Denmark). *Geochimica et Cosmochimica Acta*, *75*, 3581–3599.
- Howarth, R. W. (1984). The ecological significance of sulfur in the energy dynamics of salt marsh and coastal marine sediments. *Biogeochemistry*, *1*, 5–27.
- Jalilehvand, F. (2006). Sulfur: Not a “silent” element any more. *Chemical Society Reviews*, *38*(18), 1256–1268.
- Jensen, H. S., Kristensen, P., Jeppesen, E., & Skytthe, A. (1992). Iron:Phosphorus ratio in surface sediment as an indicator of phosphate release from aerobic sediments in shallow lakes. *Hydrobiologia*, *235-236*(1), 731–743.
- Jørgensen, B. B. (1990). A thiosulfate shunt in the sulfur cycle of marine sediments. *Science*, *249*, 152–154.
- Kohnen, M. E. L., Sinnighe Damste, J. S., ten Haven, H. L., & de Leeuw, J. W. (1989). Early incorporation of polysulfides in sedimentary organic matter. *Nature*, *341*, 640–641.
- Laskov, C., Herzog, C., Lewandowski, J., & Hupfer, M. (2007). Miniaturized photometrical methods for the rapid analysis of phosphate, ammonium, ferrous iron, and sulfate in pore water of freshwater sediments. *Limnology & Oceanography Methods*, *5*(1), 63–71.
- Luther, G. W., Ferdelman, T. G., Kostka, J. E., Tsamakis, E. J., & Church, T. M. (1991). Temporal and spatial variability of reduced sulfur species (FeS_2 , $\text{S}_2\text{O}_3^{2-}$) and porewater parameters in salt marsh sediments. *Biogeochemistry*, *14*, 57–88.
- Luther, G. W., Glazer, B. T., Hohmann, L., Popp, J. I., Taillefert, M., Rozan, T. F., Brendel, P. J., Theberge, S. M., & Nuzzio, D. B. (2001). Sulfur speciation monitored in situ with solid state gold amalgam voltammetric microelectrodes: Polysulfides as a special case in sediments, microbial mats and hydrothermal vent waters. *Journal of Environmental Monitoring*, *3*, 61–66.
- Manceau, A., & Nagy, K. L. (2012). Quantitative analysis of sulfur functional groups in natural organic matter by XANES spectroscopy. *Geochimica et Cosmochimica Acta*, *99*, 206–223.
- Meyers, P. A., & Ishiwatari, R. (1993). Lacustrine organic geochemistry—an overview of indicators of organic matter sources and diagenesis in lake sediments. *Organic Geochemistry*, *20*(7), 867–900.
- Muyzer, G., & Stams, A. J. (2008). The ecology and biotechnology of sulphate-reducing bacteria. *Nature Reviews Microbiology*, *6*, 441–454.
- Naylor, C., Davison, W., Motelica-Heino, M., Van, D. B. G. A., & Van, D. H. L. M. (2004). Simultaneous release of sulfide with Fe, Mn, Ni and Zn in marine harbour sediments measured using a combined metal/sulfide DGT probe. *Science of the Total Environment*, *328*, 275–286.
- Newville, M. (2001). IFEFFIT: Interactive XAFS analysis and FEFF fitting. *Journal of Synchrotron Radiation*, *8*, 322–324.
- Nguyen-Thanh, D., & Bandosz, T. J. (2005). Activated carbons with metal containing bentonite binders as adsorbents of hydrogen sulfide. *Carbon*, *43*, 359–367.
- Panther, J. G., Bennett, W. W., Welsh, D. T., & Teasdale, P. R. (2014). Simultaneous measurement of trace metal and oxyanion concentrations in water using diffusive gradients in thin films with a Chelex-Metsorb mixed binding layer. *Analytical Chemistry*, *86*, 427–434.
- Prietzl, J., Thieme, J., Neuhäusler, U., Susini, J., & Kögel-Knabner, I. (2003). Speciation of sulphur in soils and soil particles by X-ray spectromicroscopy. *European Journal of Soil Science*, *54*, 423–433.
- Prietzl, J., Thieme, J., Salomé, M., & Knicker, H. (2007). Sulfur K-edge XANES spectroscopy reveals differences in sulfur

- speciation of bulk soils, humic acid, fulvic acid, and particle size separates. *Soil Biology & Biochemistry*, 39, 877–890.
- Prietzl, J., Thieme, J., & Salome, M. (2010). Assessment of sulfur and iron speciation in a soil aggregate by combined S and Fe micro-XANES: Microspatial patterns and relationships. *Journal of Synchrotron Radiation*, 17, 166–172.
- Pyzik, A. J., & Sommer, S. E. (1981). Sedimentary iron monosulfides: Kinetics and mechanism of formation. *Geochimica et Cosmochimica Acta*, 45, 687–698.
- Rickard, D. (1995). Kinetics of FeS precipitation: Part 1. Competing reaction mechanisms. *Geochimica et Cosmochimica Acta*, 59, 4367–4379.
- Rickard, D. (1997). Kinetics of pyrite formation by the H₂S oxidation of iron (II) monosulfide in aqueous solutions between 25 and 125° C: The rate equation. *Geochimica et Cosmochimica Acta*, 61, 115–134.
- Rickard, D., & Luther, G. W. (1997). Kinetics of pyrite formation by the H₂S oxidation of iron (II) monosulfide in aqueous solutions between 25 and 125° C: The mechanism. *Geochimica et Cosmochimica Acta*, 61, 135–147.
- Risgaard-Petersen, N., Revil, A., Meister, P., & Nielsen, L. P. (2012). Sulfur, iron, and calcium cycling associated with natural electric currents running through marine sediments. *Geochimica et Cosmochimica Acta*, 92, 1–13.
- Solomon, D., Lehmann, J., Zarruk, K. K., Dathe, J., Kinyangi, J., Liang, B., & Machado, S. (2011). Speciation and long- and short-term molecular-level dynamics of soil organic sulfur studied by X-ray absorption near-edge structure spectroscopy. *Journal of Environmental Quality*, 40, 704–718.
- Stockdale, A., Davison, W., & Zhang, H. (2009). Micro-scale biogeochemical heterogeneity in sediments: A review of available technology and observed evidence. *Earth Science Reviews*, 92(1–2), 81–97.
- Stumm, W., & Baccini, P. (1978). Man-made chemical perturbation of lakes. In A. Lerman (Ed.), *Lakes: Chemistry, Geology, Physics* (pp. 91–126). New York: Springer-Verlag.
- Thamdrup, B. (2000). Bacterial manganese and iron reduction in aquatic sediments. *Advances in Microbial Ecology*, 16, 41–84.
- Urban, N., Brezonik, P., Baker, L., & Sherman, L. (1994). Sulfate reduction and diffusion in sediments of little rock Lake, Wisconsin. *Limnology & Oceanography*, 39, 797–815.
- Vairavamurthy, A., Zhou, W., Eglinton, T., & Manowitz, B. (1994). Sulfonates: A novel class of organic sulfur compounds in marine sediments. *Geochimica et Cosmochimica Acta*, 58, 4681–4687.
- Wang, J., Chen, J., Ding, S., Guo, J., Christopher, D., Dai, Z., & Yang, H. (2016). Effects of seasonal hypoxia on the release of phosphorus from sediments in deep-water ecosystem: A case study in Hongfeng lake, Southwest China. *Environmental Pollution*, 219, 258–265.
- Wijsman, J. W., Middelburg, J. J., Herman, P. M., Böttcher, M. E., & Heip, C. H. (2001). Sulfur and iron speciation in surface sediments along the northwestern margin of the Black Sea. *Marine Chemistry*, 74, 261–278.
- Xia, K., Weesner, F., Bleam, W. F., Helmke, P. A., Bloom, P. R., & Skyllberg, U. L. (1998). Xanes studies of oxidation states of sulfur in aquatic and soil humic substances. *Soil Science Society of America Journal*, 62(5), 1240–1246.
- Xu, D., Chen, Y., Ding, S., Sun, Q., Wang, Y., & Zhang, C. (2013). Diffusive gradients in thin films technique equipped with a mixed binding gel for simultaneous measurements of dissolved reactive phosphorus and dissolved iron. *Environmental Science & Technology*, 47, 10477–10484.
- Yao, W., & Millero, F. J. (1996). Oxidation of hydrogen sulfide by hydrous Fe(III) oxides in seawater. *Marine Chemistry*, 52, 1–16.
- Zeng, T., Arnold, W. A., & Toner, B. M. (2013). Microscale characterization of sulfur speciation in lake sediments. *Environmental Science & Technology*, 47, 1287–1296.
- Zhu, M. X., Chen, L. J., Yang, G. P., Huang, X. L., & Ma, C. Y. (2014). Humic sulfur in eutrophic bay sediments: Characterization by sulfur stable isotopes and K-edge XANES spectroscopy. *Estuarine Coastal & Shelf Science*, 138, 121–129.